The Hsf1-sHsp cascade has pan-antiviral activity in mosquito cells

Jieqiong Qu†, Michelle Schinkel†, Lisa Chiggiato, Samara Rosendo Machado, Gijs J. Overheul, Pascal Miesen, Ronald P. van Rij *

Department of Medical Microbiology, Radboud University Medical Center, P.O. Box 9101, 6500 HB Nijmegen, The Netherlands

† These authors contributed equally to this study

* For correspondence: Ronald.vanRij@radboudumc.nl

Abstract

Aedes mosquitoes transmit pathogenic arthropod-borne (arbo) viruses, putting nearly half the world's population at risk. Blocking virus replication in mosquitoes is a promising approach to prevent arbovirus transmission, the development of which requires in-depth knowledge of virus-host interactions and mosquito immunity. By integrating multi-omics data, we find that heat shock factor 1 (Hsf1) regulates eight small heat shock protein (sHsp) genes within one topologically associated domain in the mosquito genome. This Hsf1-sHsp cascade acts as an early response against chikungunya virus (CHIKV) infection and shows pan-antiviral activity in cell lines of three vector mosquitoes, *Aedes aegypti*, *Aedes albopictus*, and *Anopheles gambiae*. Our comprehensive *in vitro* data suggest that Hsf1 could serve as a promising target for the development of novel intervention strategies to limit arbovirus transmission by mosquitoes.

Author summary

With the unprecedented geographical expansion of *Aedes* mosquitoes, frequent resurgences of arbovirus epidemics have posed a significant health and economic burden. In light of this challenge, we have pursued an approach that seeks to find novel targets to block virus transmission at the mosquito stage. Through our multi-omics investigation, we have identified a new antiviral cascade, Hsf1-sHsp, that exhibits broad antiviral activity against alphaviruses and a flavivirus in cells of three vector mosquito species, *Aedes aegypti*, *Aedes albopictus*, and *Anopheles gambiae*. Given the pan-antiviral activity of the Hsf1-sHsp cascade, our findings have significant implications for understanding arbovirus-vector interactions and identifies Hsf1 as a putative target for novel approaches to prevent arbovirus transmission.

Introduction

Aedes mosquitoes are the primary vectors of arthropod-borne (arbo) viruses [1] that pose significant health and economic burden to humans [2-4]. Dengue virus (DENV) alone causes approximately 400 million infections and 20,000 deaths annually [5]. Recent outbreaks of chikungunya virus (CHIKV) in Europe and the Americas have also garnered significant attention [6-11]. With the continued resurgence of arboviruses and their unprecedented geographical spread over the past years, there is a pressing need for novel strategies to prevent and mitigate future outbreaks.

Arbovirus transmission occurs primarily through a horizontal cycle between blood-feeding arthropod vectors, such as mosquitoes, and vertebrate hosts. Female mosquitoes ingest viruses during a blood meal from an infected host and then transfer viruses into a naïve host through biting [12, 13]. Blocking virus transmission at the mosquito stage, rather than solely targeting the virus in human hosts, constitutes a promising, alternative approach to prevent arbovirus spread [14]. The development of such approaches requires in-depth knowledge of mosquito antiviral immunity.

Our current understanding of the insect immune system is largely informed by studies in *Drosophila melanogaster* [15-18], where the RNA interference (RNAi) pathway serves as a major antiviral response that degrades viral RNA and inhibits replication [19-21]. Innate immune signaling pathways, specifically the NF-κB (Toll and IMD) and JAK-STAT, have also been implicated in antiviral defense [16, 23]. However, *Drosophila* does not recapitulate mosquito specific processes such as virus acquisition and transmission via blood-feeding [12, 13, 15, 23]. It is therefore crucial to study immunity against arboviruses in relevant species, such as *Ae. aegypti*, the primary vector of the urban virus transmission cycle [24, 25].

RNAi has been identified as a major antiviral response in *Ae. aegypti* mosquitoes, for example, against CHIKV [26], Zika virus (ZIKV) [27, 28], DENV [29, 30], and Sindbis virus (SINV) [31]. In contrast, the role of classical innate immune pathways is less well-defined and seems to be virus dependent [22, 32-36]. For instance, ZIKV infection activates the Toll pathway, while DENV infection activates

both the Toll and JAK-STAT pathways [32-34]. Activation of the Toll and JAK-STAT pathways by depleting pathway-specific negative regulators Cactus and PIAS, respectively, suppresses ZIKV infection [32]. On the other hand, activation of the IMD pathway by silencing of Caspar did not affect ZIKV infection [32], but impaired SINV replication [35]. Additionally, stimulation with either heat inactivated *Escherichia coli* to activate the JAK-STAT and IMD pathways or *Bacillus subtilis* to activate Toll pathway had no effect on CHIKV replication [26], suggesting unknown antiviral mechanisms yet to be discovered.

To investigate the transcriptional responses of *Ae. aegypti* to viral infection, we conducted a time-course RNA-seq experiment upon CHIKV infection. Our combined analyses of RNA-seq and chromatin profiling data revealed an early-responsive cascade, consisting of heat shock factor 1 (Hsf1) driving the expression of eight small heat shock proteins (sHsps). This Hsf1-sHsp cascade displayed conserved pan-antiviral activities in *in vitro* experiments on three vector mosquitoes. As such, our data suggest that Hsf1 serves as a promising target for the development of new intervention strategies to control arbovirus transmission by mosquitoes.

Results

The Hsf1-sHsp cascade acts as an early response to CHIKV infection

To uncover novel components involved in antiviral defense in *Aedes* mosquitoes, we performed a time-course RNA-seq experiment to determine differentially expressed genes (DEgenes) upon CHIKV infection of *Ae. aegypti* Aag2 cells at 4, 8, and 48 hours post-infection (hpi) (Fig 1A and Table S1). The CHIKV strain that emerged during the 2005–2006 outbreaks, which acquired a mutation (A226V) in the E1 envelope glycoprotein, was used in this study [37]. A multiplicity of infection (MOI) of 5 was used to ensure that the vast majority of cells are synchronously infected. Pilot RT-qPCR indicated that CHIKV RNA strongly increased from 4 hpi onwards (Fig S1A), mirroring the dynamics of CHIKV RNA reads in our RNA-seq data (Fig S1B). At 4 hpi, only a single DEgene was detected (*AAEL000080*, encoding a putative phosphoenolpyruvate carboxykinase), which was downregulated at 8 hpi (Fig 1A). We observed major transcriptional changes at 8 hpi and 48 hpi, which we termed the early and late responses to CHIKV infection, respectively. The late response was more pronounced, with eight upregulated and 51 downregulated genes (Fig 1A), and KEGG pathway analysis suggested that downregulated DEgenes were mainly involved in glycolysis, which we have reported before [38]. In contrast, the early response was modest, with two downregulated and 19 upregulated genes, which were enriched for genes encoding HSP20-like chaperones (Fig 1A). Protein domain analysis revealed four genes encoding heat shock protein 70 (Hsp70) and eight genes encoding small heat shock proteins (sHsps) (Fig 1B), which function to prevent protein aggregation and to help cells to survive stressful conditions [39].

While Hsp70 is involved in distinct steps of the viral cycle of dengue and Zika virus in mosquito cells, including entry, RNA replication, and virion assembly [40, 41], the role of sHsps during virus infection is largely unknown [42, 43]. Inspecting the genomic distribution of these sHsp genes, we found that all eight sHsps are encoded within one Topologically Associated Domain (TAD) deduced from Hi-C seq data [44] (Fig 1C), suggesting that these sHsp genes are likely to be coordinately regulated by the

same cis-regulatory network [45, 46]. To further study the regulation of sHsp gene expression within this TAD, we mapped our chromatin profiling data from Aag2 cells [47], and performed motif scan within open chromatin regions defined by the Assay for Transposase-Accessible Chromatin with sequencing (ATAC-seq). We found the DNA binding motif of the transcription factor heat shock factor 1 (Hsf1) to be highly enriched at promoter regions of these eight sHsp genes, but not at other genes within the same TAD (Fig 1D). These regions were also marked by active histone marks H3K4me3 and H3K27ac, as well as RNA polymerase II occupancy, indicating active transcription [48, 49]. These findings together suggest that Hsf1 is the transcription factor that regulates sHsp gene expression. To experimentally test this hypothesis, we RNAi silenced *Hsf1*, and indeed, the induction of all eight *sHsps* upon CHIKV infection was significantly diminished (Fig 1E). Hence, the Hsf1-sHsp cascade functions as an early transcriptional response to CHIKV infection in Aag2 cells.

The Hsf1-sHsp cascade displays anti-CHIKV activity

To explore the antiviral potential of the identified Hsf1-sHsp axis, we silenced *Hsf1* using RNAi and observed elevated CHIKV RNA levels at 8 hpi (Fig 2A). sHsp genes share high similarity at the nucleotide level, we therefore used two sets of dsRNA targeting the conserved Hsp20 domain to knock down all 8 *sHsp* genes and observed significantly increased CHIKV RNA copies at 8 hpi (Fig 2B). In contrast, knockdown of *Hsp70* did not affect CHIKV replication (Fig 2C), although we cannot exclude that Hsp70 may affect other stages of the viral life cycle [40, 41]. These results collectively suggest that the Hsf1-sHsp axis has antiviral activity against CHIKV infection.

We then modulated the activity of Hsf1 with either the small molecule inhibitor KRIBB11 [50] or the activator hsfa1 [51] (Figs 3A-B). KRIBB11 inhibits Hsf1-dependent recruitment of positive Transcription Elongation Factor b to the promoters of target genes, thereby blocking gene activation [50]. KRIBB11 treatment significantly downregulated most *sHsp* genes after 12 h, although this effect got weaker after 24 h. The precise mechanism by which hsfa1 activates Hsf1 remains unclear [51].

124 We observed strong activation of *sHsp* genes following hsfa1 treatment at both 12 h and 24 h. To
125 further validate our findings, we included another compound, Direct Targeted Hsf1 InhiBitor (DTHIB),
126 reported as a direct human Hsf1 inhibitor by stimulating the degradation of nuclear Hsf1 [52].
127 Unexpectedly, DTHIB treatment activated *sHsp* expression in Aag2 cells at both 12 h and 24 h, similar
128 to hsfa1 (Figs 3A-B). Thus, DTHIB acts as an Hsf1 activator rather than an inhibitor in mosquito cells.
129 Subsequently, we assessed the impact of Hsf1 modulation on CHIKV infection using the
130 aforementioned compounds (Figs 3C-D). At 12 hpi, KRIBB11 treatment did not affect *Hsf1*
131 expression, but led to more than 5-fold increase of viral RNA levels in Aag2 cells (Fig 3C), a trend that
132 remained concordant at 24 hpi (Fig 3D). While the expression of most *sHsp* genes was significantly
133 reduced with KRIBB11 treatment, counterintuitively, we observed de-repression or even activation
134 of some *sHsps*, such as *AAEL013346*, *AAEL013349*, and *AAEL013351* at 12 hpi, which is likely a
135 secondary effect of increased CHIKV replication (Fig 3C). Hsfa1 treatment significantly increased *Hsf1*
136 expression and strongly activated all eight *sHsp* genes, leading to about a 25-fold reduction in CHIKV
137 copies at 12 hpi and a 10-fold reduction at 24 hpi (Figs. 3C-D). In contrast, DTHIB did not affect *Hsf1*
138 expression at 12 hpi, but still elevated *sHsp* genes and consequently repressed CHIKV replication (Fig
139 3C). These findings align with our RNAi experiments, reinforcing the antiviral role of sHsps.
140

141 **The Hsf1-sHsp cascade affects an early, post-entry stage of the viral replication cycle**

142 To determine which stage of the CHIKV life cycle is affected by the Hsf1-sHsp cascade, we performed
143 time-of-addition assays in Aag2 cells (Fig 4A). DMSO treated cells were harvested at each indicated
144 time point to establish a reference virus replication curve. When the Hsf activator hsf1a was added
145 at time points before inoculation and up to 4 hpi, CHIKV replication was strongly inhibited (Fig 4B).
146 This observation indicates that hsfa1 affects a critical step occurring around 4 hpi but does not
147 impact earlier stages, such as the virus attachment or entry step, which typically occur within 1 hour
148 after inoculation [53]. After 4 hpi, both positive and negative sense viral RNA copies became

149 detectable, and the inhibitory effect of hsf1a on CHIKV replication began to gradually diminish (Fig
150 4C). This indicates that the Hsf1-sHsp cascade interacts with the early stage of CHIKV RNA replication
151 but does not affect subsequent stages. To validate this time window, we performed a
152 time-of-addition assay with the inhibitor KRIBB11 at 2, 4, 6, 8, 10 hpi, which showed the same
153 pattern: a gradual loss of activation of CHIKV replication after 4 hpi (Figs 4D-E). Together, these
154 results demonstrate that the Hsf1-sHsp cascade likely reduces early CHIKV replication.
155
156 **The Hsf1-sHsp cascade showed pan-antiviral activity**
157 We next investigated the effect of the Hsf1-sHsp cascade on replication of other alphaviruses in Aag2
158 cells, including SINV (AR339 strain), the insect-specific Agua Salud alphavirus (ASALV), and the
159 flavivirus DENV (serotype 2). Consistently, KRIBB11 treatment led to increased virus replication for
160 SINV and ASALV, whereas hsfa1 treatment significantly reduced virus replication for SINV, ASALV and
161 DENV (Figs 5A-C). We extended our findings to *in vitro* experiments of other mosquito species and
162 confirmed the antiviral property of the Hsf1-sHsp cascade in several natural virus-vector
163 combinations [54, 55], such as CHIKV in *Aedes albopictus* U4.4 cells (Fig 5D) and C6/36 cells (Fig 5E),
164 and O'nyong-nyong (ONNV) in *Anopheles gambiae* Mos55 cells (Fig 5F). The fact that the heat shock
165 response was antiviral in both U4.4 cells and the RNAi-deficient C6/36 cells indicates that the
166 Hsf1-sHsps cascade functions independently of RNAi. Collectively, these results suggest that the
167 newly defined Hsf1-sHsp pathway displays a pan-antiviral role in cells from all three tested mosquito
168 species. As such, the upstream transcription factor, Hsf1, serves as a potential target for developing
169 antiviral interventions in mosquitoes.
170

171 **Discussion**

172 Our combined analyses of RNA-seq and epigenetic profiling data revealed an early-responsive
173 Hsf1-sHsp cascade activated upon CHIKV infection, which we found to have broad *in vitro* antiviral
174 activity against alphaviruses and a flavivirus in cell lines of three vector mosquito species: *Ae.*
175 *aegypti*, *Ae. albopictus*, and *An. gambiae*. Overall, our work uncovers a novel antiviral cascade
176 Hsf1-sHsp and identifies Hsf1 as a potential target for developing transmission-blocking strategies
177 against arboviruses at the mosquito stage.

178 While RNAi is a well-established antiviral mechanism in mosquito vectors, it is becoming evident that
179 inducible signaling pathways are of vital importance as well. In addition to the classical Toll, IMD, and
180 JAK-STAT pathways, Wnt, mTOR, Ras/ERK, JNK pathways, and the Hsf1-sHsp cascade identified in this
181 study, have been implicated in antiviral host defense [22, 32, 34, 35, 56-58]. Our time-course
182 RNA-seq data revealed that the temporal activation of signaling pathways and associated genes is
183 precisely regulated, with *sHsp* gene activation mainly restricted to the early stage of CHIKV infection
184 and not detectable during later stages. In line with our findings, published RNA-seq data from an *in*
185 *vivo* study of *Ae. aegypti* mosquitoes showed a similar pattern, with a higher induction of *sHsp*
186 expression at the early stage (3 dpi) than at the late stage (7 dpi) of CHIKV infection [42]. In
187 comparison to the well-studied role of Hsp70 at various stages of the viral cycle [40, 41, 59, 60], few
188 studies analyzed the role of sHsps in viral infection. This gap in research may be due to the transient
189 activation patterns of sHsp genes during the early stages of virus infection. Their activation is highly
190 dependent on the virus infection dynamics, making it challenging to capture this fleeting time
191 window. In addition, arboviruses need to overcome tissue barriers to establish a persistent infection
192 of the mosquito. Consequently, the infection state of different tissues or body parts can vary
193 significantly. This may explain why only two studies reported the activation of sHsps [42, 43], among
194 the many transcriptome studies that have been conducted in the context of CHIKV infection in *Aedes*

195 mosquitoes [22, 42, 43, 61-64]. Single-cell RNA-seq has emerged as a powerful tool to address the
196 heterogeneity of sHsp activation in a tissue-specific or even cell-specific context.
197 To gain deeper insights into the regulation of *sHsp* genes, we performed integrative analyses of 3D
198 chromatin conformation (Hi-C seq) and chromatin profiling data (ATAC-seq and ChIP-seq) and
199 identified Hsf1 as the upstream transcription factor that regulates expression of eight *sHsp* genes
200 within one TAD. Targeting the transcription factor Hsf1, rather than individual downstream genes, is
201 expected to be more effective for antiviral control. Together, our multi-omics analysis strategy
202 demonstrates its power in discovering novel antiviral signaling pathways, which can be applied to
203 further investigate virus-vector interactions in different tissues, in other mosquito species, and in
204 other arbovirus infections.
205 The mechanism underlying the antiviral activity of the Hsf1-sHsp cascade remains largely elusive. Our
206 time-of-addition assays suggest that the response inhibits an early post-entry stage of the viral
207 replication cycle. As Hsf1 activation led to a broad antiviral effect in three vector mosquitoes, it is
208 likely that the Hsf1-sHsp cascade interacts, either directly or indirectly, with a common viral protein
209 feature or a conserved host protein complex. It has been suggested that sHsps maintain protein
210 homeostasis by binding proteins in non-native conformations, thereby preventing substrate
211 aggregation [65]. The fact that a wide range of proteins is protected from precipitation suggests that
212 sHsps may act rather promiscuously, similarly to the molecular chaperone Hsp70 [65-69]. It will be of
213 great interest to profile sHsp associated proteins using proteomic approaches to identify sHsp client
214 proteins and shed light on its antiviral mechanism.
215 To sum up, we identified the Hsf1-sHsp cascade as a novel antiviral mechanism in cell models of
216 different mosquitoes and propose Hsf1 as a potential target for developing arbovirus-blocking
217 interventions. Considering the pan-antiviral activity of the Hsf1-sHsp cascade, our findings may open
218 the way for the development of a broad-spectrum drug to prevent arbovirus transmission.

219 ## Materials and Methods

220 **Cell lines**

221 *Ae. aegypti* Aag2 cells were kindly provided by Raul Andino (University of California San Francisco),
222 *Ae. albopictus* U4.4 cells by Gorben Pijlman (Wageningen University), and C6/36 cells by Sandra
223 Junglen (Charité, Berlin). These cell lines were grown in Leibovitz's L-15 medium (Gibco 21083-027)
224 supplemented with 10% fetal bovine serum (Sigma F7524-500ML), 50 U/ml Penicillin, 50 µg/mL
225 Streptomycin (Gibco 15070-063), 1x non-essential Amino Acids (Gibco 11140-035), and 2% Tryptose
226 phosphate broth solution (Sigma T8159-100ML). *An. gambiae* Mos55 cells were kindly provided by
227 Jason L. Rasgon (The Pennsylvania State University) and were grown in Schneider's insect medium
228 (Gibco 21720024) supplemented with 10% fetal bovine serum, 50 U/ml Penicillin, and 50 µg/mL
229 Streptomycin. Mosquito cell lines were cultured at 28°C without CO_2. BHK-15 (kind gift of Jolanda
230 Smit, University of Groningen) and BHK-21 cells (ATCC) were grown in Dulbecco's modified Eagle
231 medium (Gibco 41965039), supplemented with 10% fetal bovine serum, 50 U/mL penicillin, and 50
232 µg/mL streptomycin. Mammalian cells were cultured at 37°C, with 5% CO_2.

233

234 **Viruses**

235 The CHIKV expression plasmid encoding the Leiden synthetic wildtype strain (LS3, GenBank:
236 JX911334.1) was kindly provided by Dr. M.J. van Hemert (Leiden University Medical Center) and viral
237 RNA was obtained by *in vitro* transcription on linearized plasmids using T7 mMessage mMachine
238 (Invitrogen AM1344) [37]. RNA was then transfected into BHK-21 to grow the infectious virus. SINV
239 AR339 strain was obtained by transfecting *in vitro* transcribed RNA from linearized plasmid pTE3' 2J
240 in BHK-21 cells [70]. ASALV (GenBank: MK959114), kindly provided by Sandra Junglen (Charité,
241 Berlin), was originally isolated from the homogenate of mosquito pool MP416 and grown in C6/36
242 cells [71]. ONNV plasmid was kindly provided by Prof. Dr. Andres Merits (University of Tartu), *in vitro*
243 transcribed, and grown in C6/36 cells [72]. DENV serotype 2 (DENV2, strain 16681) was provided by

244 Beate Kümmerer (University of Bonn) and stocks were prepared on C6/36 cells. For the
245 quantification of viral stocks, CHIKV, SINV, and ONNV were titrated by end-point dilution on BHK-21
246 cells, DENV2 was titrated on BHK-15 cells, and ASALV was titrated on C6/36 cells. A day before the
247 titration, $1x10^4$ mammalian or $5x10^4$ C6/36 cells were seeded per well in a 96-well flat bottom plate.
248 A 10-fold serial dilution of virus samples was added to the cells in quadruplicate for the titration.
249 After an incubation of 5 days, cells were inspected for cytopathic effect. The virus titer was
250 calculated according to the Reed and Muench method [73].
251
252 **RNAi in mosquito cells**
253 PCR products flanked by T7 promoter sequences at both ends were *in vitro* transcribed by T7
254 polymerase to produce dsRNA. These PCR products were *in vitro* transcribed using a homemade T7
255 RNA polymerase. For the formation of double-stranded RNA, the reactions were heated to 90 °C for
256 10 minutes and then allowed to gradually cool to room temperature and RNA was purified using the
257 GenElute Mammalian Total RNA kit (Sigma RTN350) according to the manufacturer's protocol. Two
258 sets of dsRNA targeting the Hsp20 domain were used to knock down *sHsp* expression (Fig 2B) and
259 two sets of dsRNA targeting the Hsp70 domain were used to knock down *Hsp70* (Fig 2C). For detailed
260 oligonucleotide information, see Table S2.
261 Aag2 cells were seeded at a density of $1.5x10^5$ cells/well in a 24-well plate, 24 h before the dsRNA
262 transfection. For each target gene, a transfection mix containing 300 µl non-supplemented L-15
263 medium, 500 ng dsRNA, and 1.3 µl X-treme GENE HP DNA transfection reagent (Roche 6366546001)
264 was prepared according to the manufacturer's recommendations. Per well, 100 µl of the transfection
265 mix was added in a dropwise manner. Cell culture medium was refreshed at 4 h post-transfection.
266 Three days post-transfection, cells were either harvested for evaluation of target gene knockdown or
267 infection with CHIKV at an MOI of 5.
268

269 **RNA isolation and RT-qPCR**

270 Aag2 cells were homogenized in RNA-Solv reagent (Omega Bio-Tek) and RNA extraction was
271 performed according to the manufacturer's instructions. Briefly, 200 µl of chloroform was added to 1
272 mL RNA-Solv reagent and thoroughly mixed. After centrifugation, the aqueous phase was collected,
273 and RNA was precipitated using isopropanol. This mix was incubated for 1 hour at 4 °C, followed by
274 centrifugation to pellet the RNA. Pellets were washed twice in 80% ethanol and dissolved in nuclease
275 free water. RNA integrity was evaluated on ethidium bromide-stained agarose gels, and RNA
276 concentration was determined using the Nanodrop ND-1000.

277 For RT-qPCR analyses, DNaseI (Ambion)-treated RNA was reverse transcribed with random hexamers
278 using the TaqMan Reverse Transcription Reagents (Invitrogen N8080234) and PCR amplified using
279 the GoTaq qPCR system (Promega A6002) on a LightCycler 480 (Roche). In RNAi experiments,
280 expression levels of target genes were normalized to the expression of the housekeeping gene
281 *lysosomal aspartic protease* (*LAP*, *AAEL006169*), and fold changes were calculated using the 2-ΔΔCT
282 method [74]. All primers are listed in Table S2.

283

284 **RNA-seq library preparation and analysis**

285 For RNA sequencing in Aag2 cells, control dsRNA (dsLuc) treated cells were infected with CHIKV at an
286 MOI of 5. The dsRNA treatment was included in the procedure to allow a better comparison of the 4
287 hpi and 8 hpi samples to the 48 hpi datasets that was generated in parallel for a previously published
288 study (PRJNA885496) [38].

289 TruSeq Stranded mRNA kit (Illumina 20020594) was used for library preparation from total RNA
290 according to the manufacturer's protocol. The prepared libraries were quantified and controlled for
291 sample quality using High Sensitivity DNA Chip on a DNA1000 Bioanalyzer (Agilent 5067-4626), and
292 the libraries were analyzed on an Illumina HiSeq 4000 sequencer (GenomEast Platform).

293 After initial quality control by FastQC [75], raw sequence reads were aligned to the reference
294 genome, *Ae. aegypti* LVP (VectorBase, release 56) and the plasmid CHIKV genome (LS3, GenBank:
295 JX911334.1, see M&M viruses), using STAR [76] with default settings. Quantification of gene
296 expression (FPKM) was performed with Cuffdiff [77]. R package DESeq2 was used for differential
297 gene expression analysis (with adjusted p value < 0.05) [78]. Genes were considered expressed if the
298 mean of the DESeq2-normalized counts (basement) was higher than 20. The R package pheatmap
299 was used to generate the heatmap for DEgenes upon CHIKV infection, which was based on z-scores
300 of normalized gene expressions ($\log_{10}$ FPKM) [79]. DEgenes are listed in Table S1.
301
302 **Bioinformatic analyses**
303 STRING was used for KEGG pathway and InterPro protein domain enrichment analysis [80]. Detailed
304 protein domain analysis was performed using InterPro [81].
305 For 3D chromatin conformation analysis, TADs were defined by analyzing Hi-C data (GSE95797) [44]
306 with HiCExplorer [82]. A cutoff of p < 0.05 was used, after correcting for multiple tests.
307 pyGenomeTracks from the deepTools package [83] was used to visualize gene expression pattern,
308 TADs, and previously published chromatin profiling data from Aag2 cells, including ATAC-seq, histone
309 mark ChIP-seq and RNA pol II ChIP-seq (GSE210270) [47]. All genome browser tracks were
310 normalized to FPKM (y-axis). Open chromatin regions were defined as ATAC-seq peaks called by
311 MACS2 with standard settings and a q value of 0.05 [84]. Homer was used for DNA motif scan on
312 ATAC-seq peaks [85].
313
314 **Compound experiment**
315 KRIBB11 (2538), Hsf1a (1890), and DTHIB (3412) were purchased from Axon Medchem. All
316 compounds were dissolved in DMSO to a final concentration of 10 mM (KRIBB11) or 100 mM (Hsf1a
317 and DTHIB) and stored at 4°C for use within one month. Mosquito cells were seeded at a density of

318 $1.5x10^5$ cells/well in a 24-well plate. Cells at 50% confluency were treated with the indicated
319 concentrations of compound or an equivalent volume of DMSO and immediately afterwards
320 inoculated with virus at the indicated MOI. Cell lysates were collected at the indicated time points
321 for RNA isolation and RT-qPCR. For the time-of-addition assay, the same procedures were followed,
322 except that the medium was replaced at 1 hpi.
323
324 **Quantification and statistical analysis**
325 RT-qPCR experiments in Figs 1–5 was performed in biological triplicate, quintuplicate, sextuplicate,
326 or octuplicate, with individual data shown as dot and the bars indicating mean ± SD. Statistical
327 differences were examined by unpaired *t*-tests in GraphPad Prism 9.
328

Acknowledgments

We thank Martijn van Hemert (Leiden University Medical Center), Sandra Junglen (Charité Universitätsmedizin Berlin), Beate Kümmerer (University of Bonn), Andres Merits (University of Tartu), Jason Rasgon (Pennsylvania State University), and Jolanda Smit (University of Groningen) for providing materials. We thank Benoit Besson, Finny Varghese, and other members of the laboratory for fruitful discussions. This work was supported by a VENI grant from the Dutch Research Council to P.M. (grant number VI.Veni.202.035) and a VICI grant from the Dutch Research Council to R.P.v.R. (grant number 016.VICI.170.090).

References

1. Souza-Neto, J.A., J.R. Powell, and M. Bonizzoni, *Aedes aegypti vector competence studies: A review.* Infection, Genetics and Evolution, 2019. **67**: p. 191-209.
2. Diagne, C., et al., *High and rising economic costs of biological invasions worldwide.* Nature, 2021: p. 1-6.
3. Weaver, S.C. and W.K. Reisen, *Present and future arboviral threats.* Antiviral research, 2010. **85**(2): p. 328-345.
4. Chibueze, E.C., et al., *Zika virus infection in pregnancy: a systematic review of disease course and complications.* Reproductive health, 2017. **14**(1): p. 1-14.
5. Brady, O.J. and S.I. Hay, *The global expansion of dengue: how Aedes aegypti mosquitoes enabled the first pandemic arbovirus.* Annual review of entomology, 2020. **65**: p. 191-208.
6. Paty, M., et al., *Large number of imported chikungunya cases in mainland France, 2014: a challenge for surveillance and response.* Eurosurveillance, 2014. **19**(28): p. 20856.
7. Venturi, G., et al., *Detection of a chikungunya outbreak in Central Italy, August to September 2017.* Eurosurveillance, 2017. **22**(39): p. 17-00646.
8. Burt, F.J., et al., *Chikungunya virus: an update on the biology and pathogenesis of this emerging pathogen.* The Lancet Infectious Diseases, 2017. **17**(4): p. e107-e117.
9. Tomasello, D. and P. Schlagenhauf, *Chikungunya and dengue autochthonous cases in Europe, 2007–2012.* Travel medicine and infectious disease, 2013. **11**(5): p. 274-284.
10. Calba, C., et al., *Preliminary report of an autochthonous chikungunya outbreak in France, July to September 2017.* Eurosurveillance, 2017. **22**(39): p. 17-00647.
11. Rocklöv, J., et al., *Using big data to monitor the introduction and spread of chikungunya, Europe, 2017.* Emerging infectious diseases, 2019. **25**(6): p. 1041.
12. Farjana, T. and N. Tuno, *Multiple blood feeding and host-seeking behavior in Aedes aegypti and Aedes albopictus (Diptera: Culicidae).* Journal of medical entomology, 2013. **50**(4): p. 838-846.
13. Manore, C.A., et al., *Defining the risk of Zika and chikungunya virus transmission in human population centers of the eastern United States.* PLoS neglected tropical diseases, 2017. **11**(1): p. e0005255.
14. Baldacchino, F., et al., *Control methods against invasive Aedes mosquitoes in Europe: a review.* Pest management science, 2015. **71**(11): p. 1471-1485.
15. Merkling, S.H. and R.P. van Rij, *Beyond RNAi: antiviral defense strategies in Drosophila and mosquito.* Journal of insect physiology, 2013. **59**(2): p. 159-170.
16. Mussabekova, A., L. Daeffler, and J.-L. Imler, *Innate and intrinsic antiviral immunity in Drosophila.* Cellular and Molecular Life Sciences, 2017. **74**(11): p. 2039-2054.
17. Kingsolver, M.B., Z. Huang, and R.W. Hardy, *Insect antiviral innate immunity: pathways, effectors, and connections.* Journal of molecular biology, 2013. **425**(24): p. 4921-4936.
18. Machado, S.R., T. van der Most, and P. Miesen, *Genetic determinants of antiviral immunity in dipteran insects–Compiling the experimental evidence.* Developmental & Comparative Immunology, 2021. **119**: p. 104010.
19. Van Rij, R.P., et al., *The RNA silencing endonuclease Argonaute 2 mediates specific antiviral immunity in Drosophila melanogaster.* Genes & development, 2006. **20**(21): p. 2985-2995.
20. Wang, X.-H., et al., *RNA interference directs innate immunity against viruses in adult Drosophila.* Science, 2006. **312**(5772): p. 452-454.

21. Galiana-Arnoux, D., et al., *Essential function in vivo for Dicer-2 in host defense against RNA viruses in drosophila.* Nature immunology, 2006. **7**(6): p. 590-597.
22. Chowdhury, A., et al., *JNK pathway restricts DENV2, ZIKV and CHIKV infection by activating complement and apoptosis in mosquito salivary glands.* PLoS pathogens, 2020. **16**(8): p. e1008754.
23. Tafesh-Edwards, G. and I. Eleftherianos, *Drosophila immunity against natural and nonnatural viral pathogens.* Virology, 2020. **540**: p. 165-171.
24. Vega-Rúa, A., et al., *High level of vector competence of Aedes aegypti and Aedes albopictus from ten American countries as a crucial factor in the spread of Chikungunya virus.* Journal of virology, 2014. **88**(11): p. 6294-6306.
25. Coffey, L.L., A.-B. Failloux, and S.C. Weaver, *Chikungunya virus–vector interactions.* Viruses, 2014. **6**(11): p. 4628-4663.
26. McFarlane, M., et al., *Characterization of Aedes aegypti innate-immune pathways that limit Chikungunya virus replication.* PLoS Negl Trop Dis, 2014. **8**(7): p. e2994.
27. Buchman, A., et al., *Engineered resistance to Zika virus in transgenic Aedes aegypti expressing a polycistronic cluster of synthetic small RNAs.* Proceedings of the National Academy of Sciences, 2019. **116**(9): p. 3656-3661.
28. Magalhaes, T., et al., *Induction of RNA interference to block Zika virus replication and transmission in the mosquito Aedes aegypti.* Insect biochemistry and molecular biology, 2019. **111**: p. 103169.
29. Franz, A.W., et al., *Engineering RNA interference-based resistance to dengue virus type 2 in genetically modified Aedes aegypti.* Proceedings of the National Academy of Sciences, 2006. **103**(11): p. 4198-4203.
30. Sánchez-Vargas, I., et al., *Dengue virus type 2 infections of Aedes aegypti are modulated by the mosquito's RNA interference pathway.* PLoS Pathog, 2009. **5**(2): p. e1000299.
31. Khoo, C.C., et al., *The RNA interference pathway affects midgut infection-and escape barriers for Sindbis virus in Aedes aegypti.* BMC microbiology, 2010. **10**(1): p. 1-12.
32. Angleró-Rodríguez, Y.I., et al., *Aedes aegypti molecular responses to Zika virus: modulation of infection by the toll and jak/stat immune pathways and virus host factors.* Frontiers in microbiology, 2017. **8**: p. 2050.
33. Xi, Z., J.L. Ramirez, and G. Dimopoulos, *The Aedes aegypti toll pathway controls dengue virus infection.* PLoS Pathog, 2008. **4**(7): p. e1000098.
34. Behura, S.K., et al., *Global cross-talk of genes of the mosquito Aedes aegypti in response to dengue virus infection.* PLoS Negl Trop Dis, 2011. **5**(11): p. e1385.
35. Barletta, A.B.F., et al., *Microbiota activates IMD pathway and limits Sindbis infection in Aedes aegypti.* Parasites & vectors, 2017. **10**(1): p. 1-9.
36. Souza-Neto, J.A., S. Sim, and G. Dimopoulos, *An evolutionary conserved function of the JAK-STAT pathway in anti-dengue defense.* Proceedings of the National Academy of Sciences, 2009. **106**(42): p. 17841-17846.
37. Scholte, F.E., et al., *Characterization of synthetic Chikungunya viruses based on the consensus sequence of recent E1-226V isolates.* PloS one, 2013. **8**(8): p. e71047.
38. Machado, S.R., et al., *The DEAD-box RNA helicase Dhx15 controls glycolysis and arbovirus replication in Aedes aegypti mosquito cells.* bioRxiv, 2022: p. 2022.06.22.497281.
39. Garrido, C., et al., *The small heat shock proteins family: the long forgotten chaperones.* The international journal of biochemistry & cell biology, 2012. **44**(10): p. 1588-1592.

40. Taguwa, S., et al., *Defining Hsp70 subnetworks in dengue virus replication reveals key vulnerability in flavivirus infection.* Cell, 2015. **163**(5): p. 1108-1123.
41. Taguwa, S., et al., *Zika virus dependence on host Hsp70 provides a protective strategy against infection and disease.* Cell reports, 2019. **26**(4): p. 906-920. e3.
42. Wimalasiri-Yapa, B.R., et al., *Temperature modulates immune gene expression in mosquitoes during arbovirus infection.* Open biology, 2021. **11**(1): p. 200246.
43. Dong, S., S.K. Behura, and A.W. Franz, *The midgut transcriptome of Aedes aegypti fed with saline or protein meals containing chikungunya virus reveals genes potentially involved in viral midgut escape.* BMC genomics, 2017. **18**: p. 1-17.
44. Dudchenko, O., et al., *De novo assembly of the Aedes aegypti genome using Hi-C yields chromosome-length scaffolds.* Science, 2017. **356**(6333): p. 92-95.
45. Nora, E.P., et al., *Spatial partitioning of the regulatory landscape of the X-inactivation centre.* Nature, 2012. **485**(7398): p. 381-385.
46. Schoenfelder, S., et al., *The pluripotent regulatory circuitry connecting promoters to their long-range interacting elements.* Genome research, 2015. **25**(4): p. 582-597.
47. Qu, J., et al., *Chromatin profiling identifies transcriptional readthrough as a conserved mechanism for piRNA cluster biogenesis in mosquitoes.* bioRxiv, 2022.
48. Stasevich, T.J., et al., *Regulation of RNA polymerase II activation by histone acetylation in single living cells.* Nature, 2014. **516**(7530): p. 272-275.
49. Hampsey, M. and D. Reinberg, *Tails of intrigue: phosphorylation of RNA polymerase II mediates histone methylation.* Cell, 2003. **113**(4): p. 429-432.
50. Yoon, Y.J., et al., *KRIBB11 inhibits HSP70 synthesis through inhibition of heat shock factor 1 function by impairing the recruitment of positive transcription elongation factor b to the hsp70 promoter.* Journal of Biological Chemistry, 2011. **286**(3): p. 1737-1747.
51. Neef, D.W., M.L. Turski, and D.J. Thiele, *Modulation of heat shock transcription factor 1 as a therapeutic target for small molecule intervention in neurodegenerative disease.* PLoS biology, 2010. **8**(1): p. e1000291.
52. Dong, B., et al., *Targeting therapy-resistant prostate cancer via a direct inhibitor of the human heat shock transcription factor 1.* Science Translational Medicine, 2020. **12**(574): p. eabb5647.
53. Hoornweg, T.E., et al., *Dynamics of chikungunya virus cell entry unraveled by single-virus tracking in living cells.* Journal of virology, 2016. **90**(9): p. 4745-4756.
54. Hubálek, Z., *Mosquito-borne viruses in Europe.* Parasitology research, 2008. **103**: p. 29-43.
55. Vanlandingham, D.L., et al., *Differential infectivities of o'nyong-nyong and chikungunya virus isolates in Anopheles gambiae and Aedes aegypti mosquitoes.* The American journal of tropical medicine and hygiene, 2005. **72**(5): p. 616-621.
56. Sanders, H.R., et al., *Sindbis virus induces transport processes and alters expression of innate immunity pathway genes in the midgut of the disease vector, Aedes aegypti.* Insect biochemistry and molecular biology, 2005. **35**(11): p. 1293-1307.
57. Liu, W.-Q., et al., *The Ras/ERK signaling pathway couples antimicrobial peptides to mediate resistance to dengue virus in Aedes mosquitoes.* PLoS neglected tropical diseases, 2020. **14**(8): p. e0008660.
58. Chen, T.-Y., et al., *Profiling transcriptional response of dengue-2 virus infection in midgut tissue of Aedes aegypti.* Frontiers in Tropical Diseases, 2021. **2**: p. 708817.

475 59. Howe, M.K., et al., *An inducible heat shock protein 70 small molecule inhibitor*
476 *demonstrates anti-dengue virus activity, validating Hsp70 as a host antiviral target.*
477 Antiviral research, 2016. **130**: p. 81-92.
478 60. Ferreira, P.G., et al., *Temperature dramatically shapes mosquito gene expression with*
479 *consequences for mosquito–Zika virus interactions.* Frontiers in microbiology, 2020. **11**:
480 p. 901.
481 61. Vedururu, R.K., et al., *RNASeq analysis of Aedes albopictus mosquito midguts after*
482 *chikungunya virus infection.* Viruses, 2019. **11**(6): p. 513.
483 62. Zhao, L., et al., *Transcriptomic analysis of Aedes aegypti innate immune system in*
484 *response to ingestion of chikungunya virus.* International Journal of Molecular Sciences,
485 2019. **20**(13): p. 3133.
486 63. Novelo, M., et al., *Dengue and chikungunya virus loads in the mosquito Aedes aegypti*
487 *are determined by distinct genetic architectures.* PLoS pathogens, 2023. **19**(4): p.
488 e1011307.
489 64. Shrinet, J., P. Srivastava, and S. Sunil, *Transcriptome analysis of Aedes aegypti in*
490 *response to mono-infections and co-infections of dengue virus-2 and chikungunya virus.*
491 Biochemical and biophysical research communications, 2017. **492**(4): p. 617-623.
492 65. Haslbeck, M., et al., *Some like it hot: the structure and function of small heat-shock*
493 *proteins.* Nature structural & molecular biology, 2005. **12**(10): p. 842-846.
494 66. Basha, E., et al., *The identity of proteins associated with a small heat shock protein*
495 *during heat stress in vivo indicates that these chaperones protect a wide range of*
496 *cellular functions.* Journal of Biological Chemistry, 2004. **279**(9): p. 7566-7575.
497 67. Vecchi, G., et al., *Proteome-wide observation of the phenomenon of life on the edge of*
498 *solubility.* Proceedings of the National Academy of Sciences, 2020. **117**(2): p. 1015-1020.
499 68. Haslbeck, M., S. Weinkauf, and J. Buchner, *Small heat shock proteins: simplicity meets*
500 *complexity.* Journal of Biological Chemistry, 2019. **294**(6): p. 2121-2132.
501 69. Dabbaghizadeh, A. and R.M. Tanguay, *Structural and functional properties of proteins*
502 *interacting with small heat shock proteins.* Cell Stress and Chaperones, 2020. **25**(4): p.
503 629-637.
504 70. Hahn, C.S., et al., *Infectious Sindbis virus transient expression vectors for studying*
505 *antigen processing and presentation.* Proceedings of the National Academy of Sciences,
506 1992. **89**(7): p. 2679-2683.
507 71. Hermanns, K., et al., *Agua Salud alphavirus defines a novel lineage of insect-specific*
508 *alphaviruses discovered in the New World.* The Journal of general virology, 2020. **101**(1):
509 p. 96.
510 72. Varghese, F.S., et al., *The antiviral alkaloid berberine reduces chikungunya virus-induced*
511 *mitogen-activated protein kinase signaling.* Journal of virology, 2016. **90**(21): p.
512 9743-9757.
513 73. Reed, L.J. and H. Muench, *A simple method of estimating fifty per cent endpoints.*
514 American journal of epidemiology, 1938. **27**(3): p. 493-497.
515 74. Livak, K.J. and T.D. Schmittgen, *Analysis of relative gene expression data using real-time*
516 *quantitative PCR and the 2− ΔΔCT method.* methods, 2001. **25**(4): p. 402-408.
517 75. Andrews, S., *FastQC: a quality control tool for high throughput sequence data*. 2010,
518 Babraham Bioinformatics, Babraham Institute, Cambridge, United Kingdom.
519 76. Dobin, A., et al., *STAR: ultrafast universal RNA-seq aligner.* Bioinformatics, 2013. **29**(1):
520 p. 15-21.

77. Trapnell, C., et al., *Differential analysis of gene regulation at transcript resolution with RNA-seq.* Nature biotechnology, 2013. **31**(1): p. 46-53.
78. Love, M.I., W. Huber, and S. Anders, *Moderated estimation of fold change and dispersion for RNA-seq data with DESeq2.* Genome Biology, 2014. **15**(12): p. 550.
79. Kolde, R., *Pheatmap: pretty heatmaps.* R package version, 2012. **1**(2): p. 726.
80. Szklarczyk, D., et al., *The STRING database in 2021: customizable protein–protein networks, and functional characterization of user-uploaded gene/measurement sets.* Nucleic acids research, 2021. **49**(D1): p. D605-D612.
81. Paysan-Lafosse, T., et al., *InterPro in 2022.* Nucleic Acids Research, 2023. **51**(D1): p. D418-D427.
82. Ramírez, F., et al., *High-resolution TADs reveal DNA sequences underlying genome organization in flies.* Nature communications, 2018. **9**(1): p. 1-15.
83. Ramírez, F., et al., *deepTools: a flexible platform for exploring deep-sequencing data.* Nucleic acids research, 2014. **42**(W1): p. W187-W191.
84. Zhang, Y., et al., *Model-based analysis of ChIP-Seq (MACS).* Genome biology, 2008. **9**(9): p. 1-9.
85. Heinz, S., et al., *Simple combinations of lineage-determining transcription factors prime cis-regulatory elements required for macrophage and B cell identities.* Molecular cell, 2010. **38**(4): p. 576-589.

541 **Figure Legends**

542

543 **Figure 1. Hsf1 activates sHsp expression during the early stage of CHIKV infection.**

544 (A) Hierarchical clustering of differentially expressed (DE) genes at 4, 8, and 48 hpi of CHIKV infection
545 (MOI = 5) in *Aedes aegypti* Aag2 cells, as quantified from RNA-seq data. DEgenes ($p < 0.05$) at each
546 time point are color labeled on the left; KEGG pathway and InterPro enrichment is shown on the
547 right. Z scores were calculated based on log-transformed Fragments per Kilobase per Million mapped
548 reads (FPKM).

549 (B) Gene structure and protein domain analysis of heat shock proteins upregulated at 8 hpi of CHIKV
550 infection. A neighbor-joining tree was constructed based on amino acid sequences (left). The $\log_2$
551 fold changes in gene expression were quantified by RNA-seq (middle). The gene structure and
552 InterPro protein domains are shown along the gene body (right).

553 (C) Hi-C interaction track with topologically associated domains (TADs) shown as horizontal blue bars
554 ($p < 0.05$).

555 (D) Genome browser tracks showing RNA-seq data of mock and CHIKV infected Aag2 cells and
556 chromatin profiling data from uninfected Aag2 cells (ATAC-seq, histone marks and RNA pol II
557 ChIP-seq) within the indicated TAD. Eight upregulated *sHsp* genes at 8 hpi are highlighted in orange,
558 other genes in gray. Predicted Hsf1 motifs are shown as green arrowheads at the bottom.

559 (E) Expression of the indicated genes in mock (-) or CHIKV (MOI = 5) infected Aag2 cells upon
560 RNAi-mediated silencing of *Hsf1* at 8 hpi. Luciferase dsRNA served as a non-targeting control (ctr).
561 RT-qPCR was performed in biological quintuplicates and shown as dots, with horizontal lines and the
562 bars indicating mean ± SD. Symbols denote statistical significance in unpaired t-tests (ns, not
563 significant, * $p < 0.05$; ** $p < 0.01$; *** $p < 0.001$).

564

565 **Figure 2. The Hsf1-sHsp axis has antiviral activity against CHIKV.**

566 RNAi silencing of *Hsf1* (A), *sHsps* (B), *Hsp70* (*AAEL017975*) (C), and quantification of CHIKV RNA
567 copies. dsRNA targeting the highly conserved Hsp20 domain was used to knock down all eight sHsp
568 genes simultaneously in (B). RT-qPCR was used to assess target gene knockdown in uninfected Aag2
569 cells (left) and to quantify CHIKV mRNA copies at 8 hpi (MOI = 5) after target gene knockdown (right)
570 in biological triplicate or quadruplicate, with luciferase dsRNA (dsLuc) serving as a non-targeting
571 control. Individual data are shown as dots, with bars indicating mean ± SD. Symbols denote statistical
572 significance in unpaired t-tests (ns, not significant, * $p < 0.05$; ** $p < 0.01$; *** $p < 0.001$).
573
574 **Figure 3. Pathway modulation using small-molecule compounds confirms the antiviral activity of**
575 **the Hsf1-sHsps axis.**
576 (A–B) Effects of Hsf1 modulation using KRIBB11 (10 µM), hsfa1 (100 µM), and DTHIB (10 µM) on *sHsp*
577 expression measured by RT-qPCR at 12 h (A) and 24 h (B). DMSO was used as control.
578 (C–D) Expression analysis of *Hsf1*, *sHsp* genes, and CHIKV RNA copies following treatment with
579 KRIBB11 (10 µM), hsfa1 (100 µM), and DTHIB (10 µM) at 12 hpi (C) and 24 hpi (D) with CHIKV (MOI =
580 5), using DMSO as a control. RT-qPCR data are presented in biological triplicate, quadruplicate, or
581 sextuplicate, displayed as dots, with bars indicating mean ± SD. Statistical significance in unpaired
582 t-tests is denoted by symbols (ns, not significant; * $p < 0.05$; ** $p < 0.01$; *** $p < 0.001$).
583
584 **Figure 4. The Hsf1-sHsp cascade affects the early stage of the CHIKV replication cycle.**
585 (A) Schematic illustration of the time-of-addition assay during CHIKV infection (MOI = 5) in Aag2 cells.
586 Cell culture medium was refreshed to wash away unbound virus particles at 1 hpi. DMSO (light gray,
587 Mock) was used to establish a virus replication curve, with samples harvested at each indicated time
588 point. hsfa1 (orange, activator) and KRIBB11 (dark gray, inhibitor) were added at specified time
589 points, and cells were harvested at 10 hpi to assess their impact on CHIKV RNA levels.

590 (B–E) The effect of hsfa1 (100 µM) (B–C) and KRIBB11 (10 µM) (D–E) on CHIKV replication was
591 assessed using RT-qPCR on positive sense (+) viral RNA (B, D) and negative sense (-) viral RNA (C, E).
592 Data are presented as means ± SD of three independent experiments, with DMSO serving as the
593 negative control to calculate the percent inhibition (B–C) and the fold increase in virus replication
594 (D–E).
595
596 **Figure 5. Pan-antiviral activity of the Hsf1-sHsp axis**
597 (A–C) Viral RNA levels in *Aedes aegypti* Aag2 cells treated with KRIBB11 (10 µM) or hsfa1 (100 µM) at
598 12 hpi of Sindbis virus (SINV, MOI = 5) (A), at 12 hpi of Agua Salud alphavirus (ASALV, MOI = 5) (B),
599 and at 72 hpi of Dengue virus (DENV, MOI = 0.01) (C).
600 (D–F) Viral RNA levels upon treatment with KRIBB11 (5 µM) and hsfa1 (100 µM) at 12 hpi of CHIKV
601 (MOI = 5) in *Aedes albopictus* U4.4 cells (D), at 12 hpi of CHIKV (MOI = 5) in *Dicer-2* deficient *Aedes*
602 *albopictus* C6/36 cells (E), at 48 hpi of o'nyong'nyong virus (ONNV, MOI = 0.5) in *Anopheles gambiae*
603 Mos55 cells (F). RT-qPCR was performed in biological quadruplicate or sextuplicate, shown as dots,
604 with the bars indicating mean ± SD. Symbols denote statistical significance in unpaired t-tests (ns, not
605 significant, * $p < 0.05$; ** $p < 0.01$; *** $p < 0.001$).
606

607 **Supporting Information Captions**

608

609 **Table S1.** Differentially expressed genes (DEgenes) upon CHIKV infection at different time points.

610 **Table S2.** oligonucleotide information.

611 **Figure S1.** (A-B) Expression of CHIKV mRNA quantified by qPCR (A) and RNA-seq (B) in mock (-) or

612 CHIKV (MOI = 5, +) infected Aag2 cells at 4, 8, and 48h. RT-qPCR and RNA-seq was performed in

613 biological triplicates shown as dots, with horizontal lines and the bars indicating mean ±SD.

614

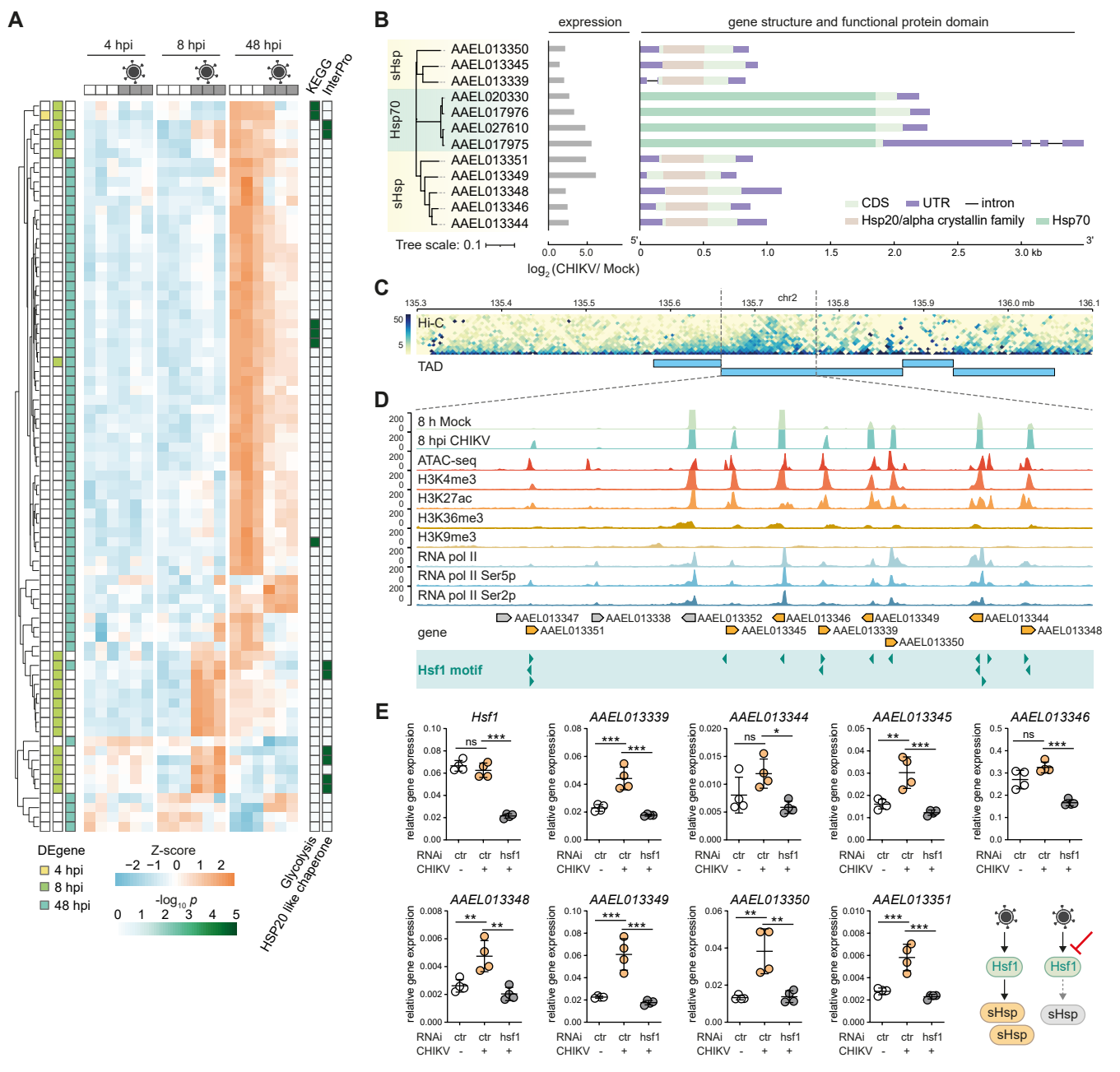
A
4 hpi
8 hpi
48 hpi
KEGG
InterPro
DEgene
4 hpi
8 hpi
48 hpi
Z-score
−2 −1 0 1 2
-log10 p
0 1 2 3 4 5
Glycolysis
HSP20 like chaperone
B
expression
gene structure and functional protein domain
sHsp
Hsp70
sHsp
AAEL013350
AAEL013345
AAEL013339
AAEL020330
AAEL017976
AAEL027610
AAEL017975
AAEL013351
AAEL013349
AAEL013348
AAEL013346
AAEL013344
Tree scale: 0.1
0.0 5.0
log2 (CHIKV/ Mock)
5'
3'
0 0.5 1.0 1.5 2.0 2.5 3.0 kb
CDS
UTR
intron
Hsp20/alpha crystallin family
Hsp70
C
135.3 135.4 135.5 135.6 135.7 chr2 135.8 135.9 136.0 mb 136.1
Hi-C
50
5
TAD
D
8 h Mock
8 hpi CHIKV
ATAC-seq
H3K4me3
H3K27ac
H3K36me3
H3K9me3
RNA pol II
RNA pol II Ser5p
RNA pol II Ser2p
200
0
gene
AAEL013347
AAEL013338
AAEL013352
AAEL013346
AAEL013349
AAEL013344
AAEL013351
AAEL013345
AAEL013339
AAEL013348
AAEL013350
Hsf1 motif
E
Hsf1
AAEL013339
AAEL013344
AAEL013345
AAEL013346
AAEL013348
AAEL013349
AAEL013350
AAEL013351
relative gene expression
ns
*
**
***
RNAi ctr ctr hsf1
CHIKV - + +
Hsf1
sHsp
sHsp

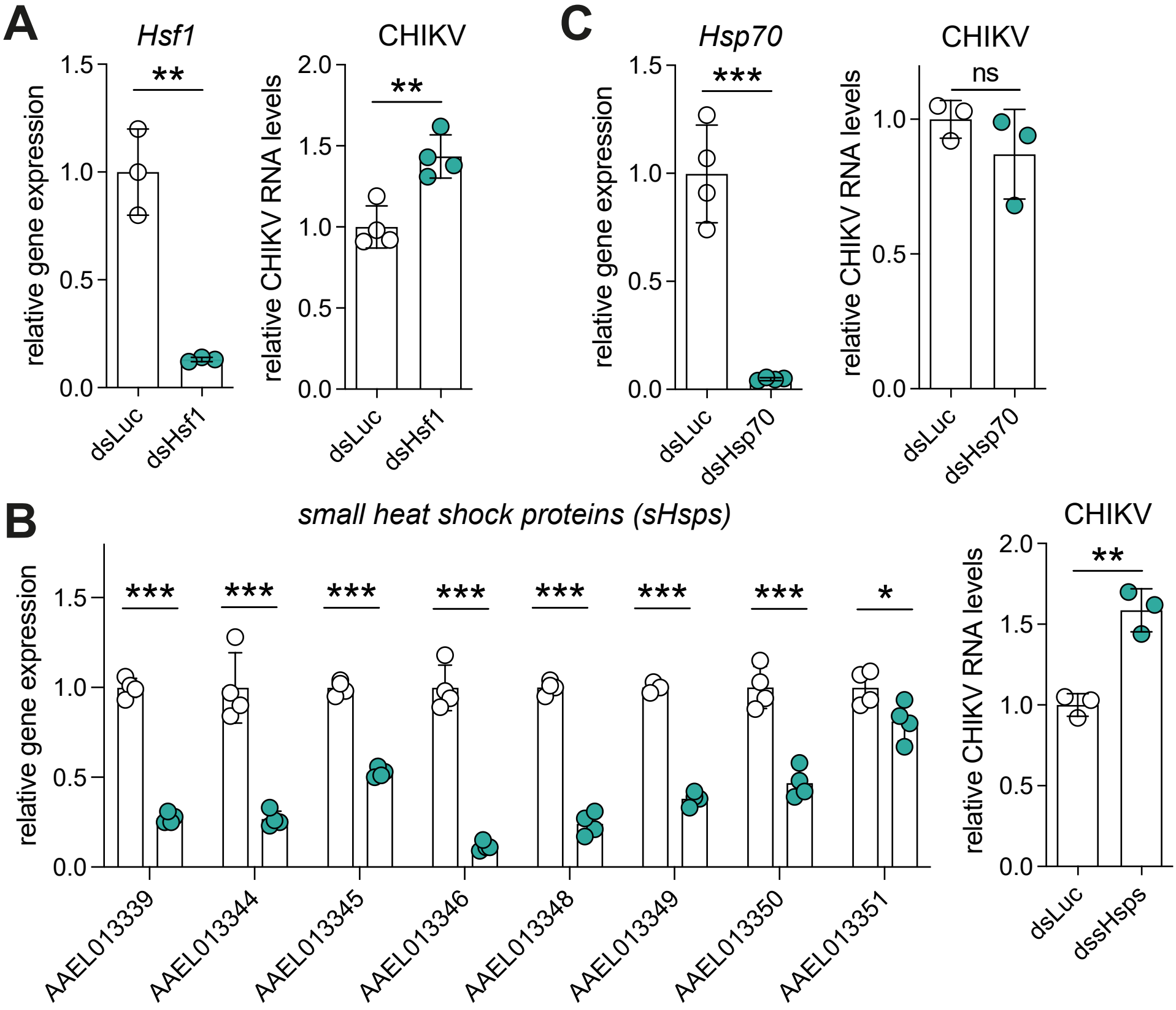
A
Hsf1
CHIKV
relative gene expression
relative CHIKV RNA levels
**
**
dsLuc
dsHsf1
C
Hsp70
CHIKV
***
ns
dsHsp70
B
small heat shock proteins (sHsps)
***
*
AAEL013339
AAEL013344
AAEL013345
AAEL013346
AAEL013348
AAEL013349
AAEL013350
AAEL013351
dssHsps

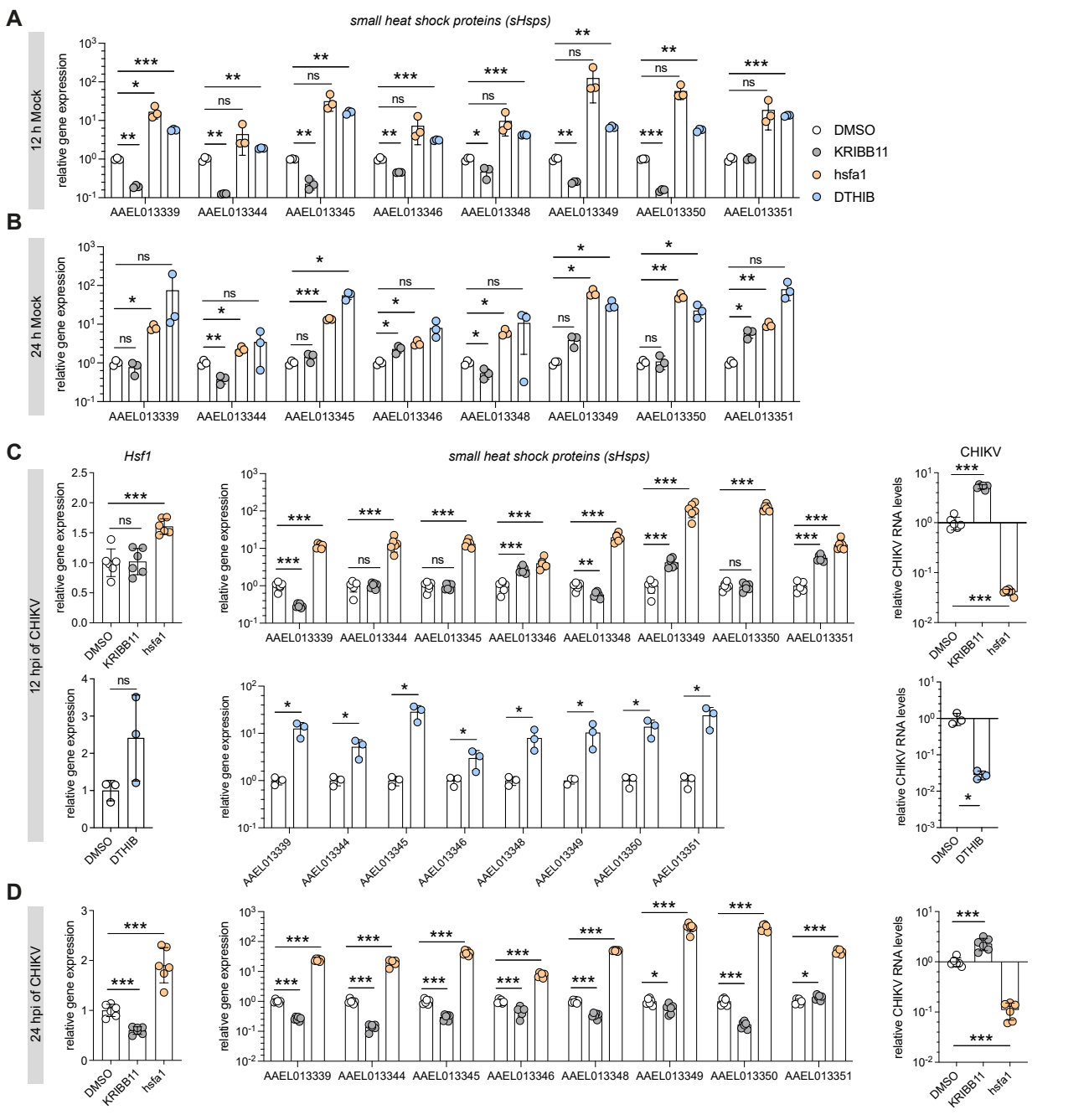
A
small heat shock proteins (sHsps)
12 h Mock
relative gene expression
AAEL013339
AAEL013344
AAEL013345
AAEL013346
AAEL013348
AAEL013349
AAEL013350
AAEL013351
DMSO
KRIBB11
hsfa1
DTHIB
B
24 h Mock
C
Hsf1
CHIKV
12 hpi of CHIKV
relative CHIKV RNA levels
D
24 hpi of CHIKV

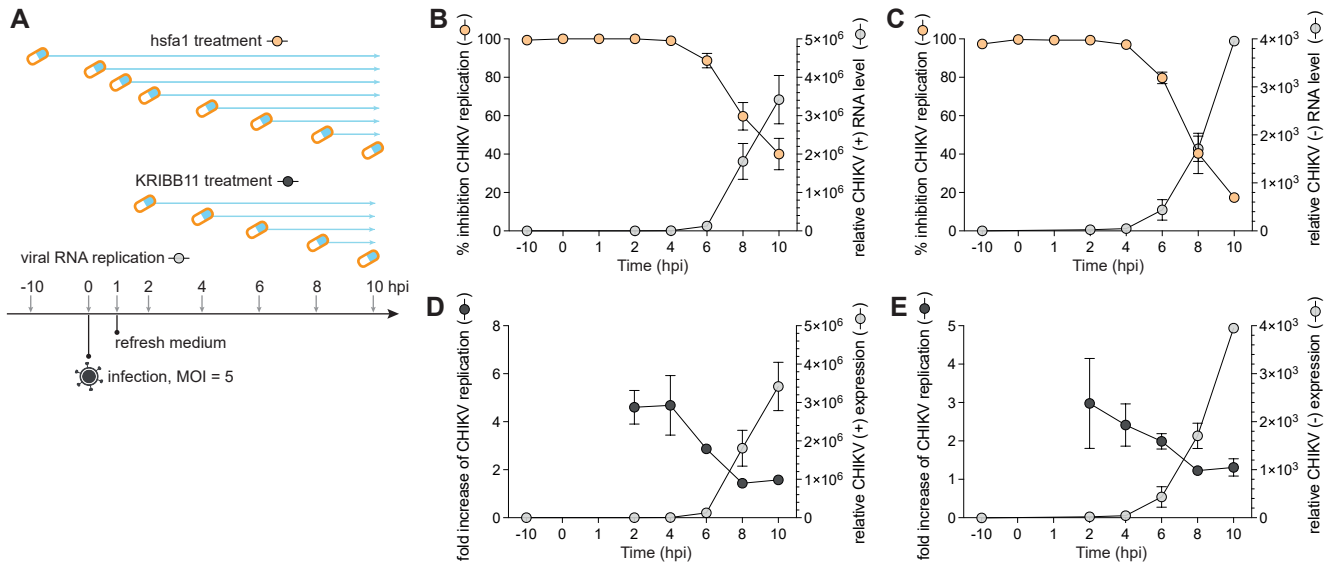
A
hsfa1 treatment
KRIBB11 treatment
viral RNA replication
-10
0
1
2
4
6
8
10 hpi
refresh medium
infection, MOI = 5
B
% inhibition CHIKV replication (-)
relative CHIKV (+) RNA level (-)
Time (hpi)
C
% inhibition CHIKV replication (-)
relative CHIKV (-) RNA level (-)
Time (hpi)
D
fold increase of CHIKV replication (-)
relative CHIKV (+) expression (-)
Time (hpi)
E
fold increase of CHIKV replication (-)
relative CHIKV (-) expression (-)
Time (hpi)

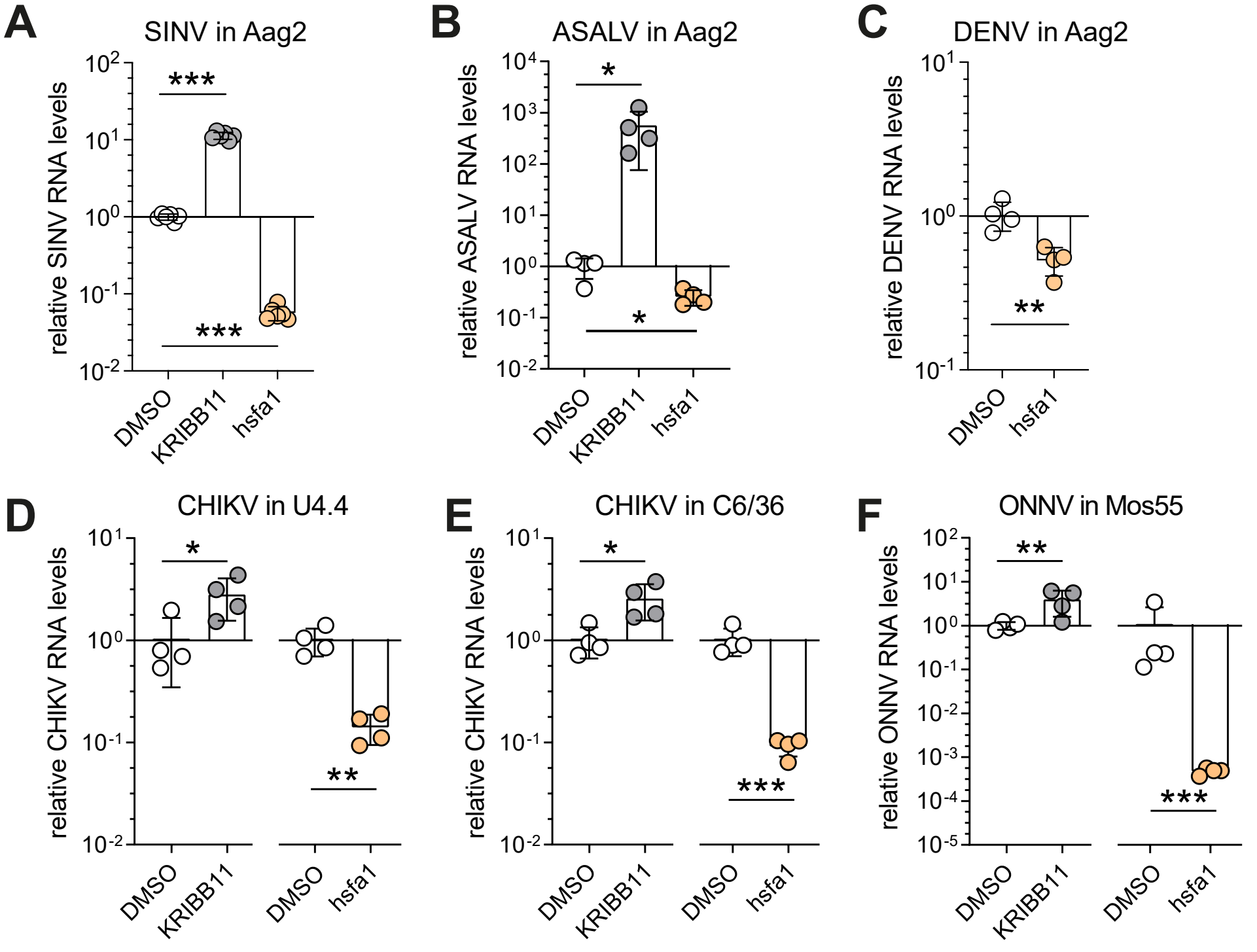
A
SINV in Aag2
relative SINV RNA levels
10^2
10^1
10^0
10^{-1}
10^{-2}
***
***
DMSO
KRIBB11
hsfa1
B
ASALV in Aag2
relative ASALV RNA levels
10^4
10^3
10^2
10^1
10^0
10^{-1}
10^{-2}
*
*
DMSO
KRIBB11
hsfa1
C
DENV in Aag2
relative DENV RNA levels
10^1
10^0
10^{-1}
**
DMSO
hsfa1
D
CHIKV in U4.4
relative CHIKV RNA levels
10^1
10^0
10^{-1}
10^{-2}
*
**
DMSO
KRIBB11
DMSO
hsfa1
E
CHIKV in C6/36
relative CHIKV RNA levels
10^1
10^0
10^{-1}
10^{-2}
*
***
DMSO
KRIBB11
DMSO
hsfa1
F
ONNV in Mos55
relative ONNV RNA levels
10^2
10^1
10^0
10^{-1}
10^{-2}
10^{-3}
10^{-4}
10^{-5}
**
***
DMSO
KRIBB11
DMSO
hsfa1